The Astrophysical Journal Letters, 848:L21 (7pp), 2017 October 20 https://doi.org/10.3847/2041-8213/aa905d

The Electromagnetic Counterpart of the Binary Neutron Star Merger LIGO/Virgo GW170817. VI. Radio Constraints on a Relativistic Jet and Predictions for Late-time Emission from the Kilonova Ejecta

K. D. Alexander[1], E. Berger[1], W. Fong[2,14], P. K. G. Williams[1], C. Guidorzi[3], R. Margutti[2], B. D. Metzger[4], J. Annis[5], P. K. Blanchard[1], D. Brout[6], D. A. Brown[7], H.-Y. Chen[8], R. Chornock[9], P. S. Cowperthwaite[1], M. Drout[10,14], T. Eftekhari[1], J. Frieman[5,8], D. E. Holz[8,11], M. Nicholl[1], A. Rest[12,13], M. Sako[6], M. Soares-Santos[5], and V. A. Villar[1]

[1] Harvard-Smithsonian Center for Astrophysics, 60 Garden Street, Cambridge, MA 02138, USA
[2] Center for Interdisciplinary Exploration and Research in Astrophysics (CIERA) and Department of Physics and Astronomy, Northwestern University, Evanston, IL 60208, USA
[3] Department of Physics and Earth Science, University of Ferrara, via Saragat 1, I-44122, Ferrara, Italy
[4] Department of Physics and Columbia Astrophysics Laboratory, Columbia University, New York, NY 10027, USA
[5] Fermi National Accelerator Laboratory, P.O. Box 500, Batavia, IL 60510, USA
[6] Department of Physics and Astronomy, University of Pennsylvania, Philadelphia, PA 19104, USA
[7] Department of Physics, Syracuse University, Syracuse NY 13224, USA
[8] Kavli Institute for Cosmological Physics, University of Chicago, Chicago, IL 60637, USA
[9] Astrophysical Institute, Department of Physics and Astronomy, 251B Clippinger Lab, Ohio University, Athens, OH 45701, USA
[10] Carnegie Observatories, 813 Santa Barbara Street, Pasadena, CA 91101, USA
[11] Enrico Fermi Institute, Department of Physics, Department of Astronomy and Astrophysics, 5640 South Ellis Avenue, Chicago, IL 60637, USA
[12] Space Telescope Science Institute, 3700 San Martin Drive, Baltimore, MD 21218, USA
[13] Department of Physics and Astronomy, The Johns Hopkins University, 3400 North Charles Street, Baltimore, MD 21218, USA
Received 2017 September 27; revised 2017 October 2; accepted 2017 October 2; published 2017 October 16

Abstract

We present Very Large Array (VLA) and Atacama Large Millimeter/submillimeter Array (ALMA) radio observations of GW170817, the first Laser Interferometer Gravitational-wave Observatory (LIGO)/Virgo gravitational wave (GW) event from a binary neutron star merger and the first GW event with an electromagnetic (EM) counterpart. Our data include the first observations following the discovery of the optical transient at both the centimeter (13.7 hr post-merger) and millimeter (2.41 days post-merger) bands. We detect faint emission at 6 GHz at 19.47 and 39.23 days after the merger, but not in an earlier observation at 2.46 days. We do not detect cm/mm emission at the position of the optical counterpart at frequencies of 10–97.5 GHz at times ranging from 0.6 to 30 days post-merger, ruling out an on-axis short gamma-ray burst (SGRB) for energies $\gtrsim 10^{48}$ erg. For fiducial SGRB parameters, our limits require an observer viewer angle of $\gtrsim 20°$. The radio and X-ray data can be jointly explained as the afterglow emission from an SGRB with a jet energy of $\sim 10^{49}$–10^{50} erg that exploded in a uniform density environment with $n \sim 10^{-4}$–10^{-2} cm^{-3}, viewed at an angle of $\sim 20°$–$40°$ from the jet axis. Using the results of our light curve and spectral modeling, in conjunction with the inference of the circumbinary density, we predict the emergence of late-time radio emission from the deceleration of the kilonova (KN) ejecta on a timescale of $\sim$5–10 years that will remain detectable for decades with next-generation radio facilities, making GW170817 a compelling target for long-term radio monitoring.

Key words: gravitational waves – relativistic processes

1. Introduction

Radio emission from binary neutron star (BNS) mergers offers a unique way to probe the energetics and geometries of their outflows, as well as their circumbinary densities. Until now, the primary way to place constraints on radio emission from BNS mergers was through rapid follow-up observations of short-duration gamma-ray bursts (SGRBs), which have been argued to result from BNS mergers (e.g., Berger 2014). A decade of SGRB radio follow-up at GHz frequencies yielded four detections and multiple upper limits (Berger et al. 2005; Soderberg et al. 2006; Fong et al. 2014, 2015), providing tight constraints on the energetics and densities of the burst environments. In particular, these observations point to low-density environments of $\sim 10^{-3}$–$0.1\,\mathrm{cm}^{-3}$, and typical beaming-corrected energies of $\sim 10^{49}$–10^{50} erg (Berger 2014; Fong et al. 2015).

The jets launched by SGRBs are collimated and highly relativistic, meaning that for their typical cosmological distances (Berger 2014) they are only detectable within a narrow range of viewing angles at early times (Fong et al. 2015). For nearby BNS mergers within 200 Mpc as expected from gravitational wave (GW) detections (Abbott et al. 2016), the emission could be detectable off-axis (Nakar & Piran 2011; Metzger & Berger 2012).

On 2017 August 17 12:41:04 UTC, the Advanced Laser Interferometer Gravitational-wave Observatory (LIGO)/Virgo detected a GW signal determined to originate from a BNS at a distance of $\sim$40 Mpc (LIGO Scientific Collaboration & Virgo Collaboration 2017a; LIGO Scientific Collaboration a Virgo Collaboration 2017b). The localization of GW170817 was spatially coincident with a weak gamma-ray transient detected by *Fermi*/GBM (Blackburn et al. 2017; Goldstein et al. 2017a, 2017b; von Kienlin et al. 2017) and *INTEGRAL* (Savchenko et al. 2017a, 2017b), termed GRB 170817A. Subsequently, an

[14] Hubble Fellow.

Table 1
Radio Observations of GW170817 and Its Host Galaxy, NGC 4993

Observatory	Start Date (UT)	Δt (days)	Avg Freq (GHz)	Freq Range (GHz)	On-source Time (hr)	Beam Size (arcsec)	Img rms (μJy/beam)[a]	Host flux density (μJy)
VLA	2017 Aug 18.1	0.57	9.7	8.0–9.0, 10.5–11.5	0.07	9.0 × 1.5	48	250 ± 55
VLA	2017 Aug 18.9	1.44	10.0	8.0–11.9	1.5	3.1 × 1.4	4.6	372 ± 17
ALMA	2017 Aug 19.9	2.41	97.5	89.5–93.5, 101.5–105.5	0.14	0.3 × 0.2	25	174 ± 34
VLA	2017 Aug 19.9	2.42	15.0	12.0–17.9	0.46	2.2 × 1.0	5.9	295 ± 18
VLA	2017 Aug 19.9	2.44	10.0	8.0–11.9	0.41	3.1 × 1.4	5.7	330 ± 11
VLA	2017 Aug 19.9	2.46	6.0	4.0–7.9	0.41	5.5 × 2.4	7.3	354 ± 12
VLA	2017 Aug 23.0	5.48	10.0	7.9–11.9	0.60	3.8 × 1.5	9.5	274 ± 22
VLA	2017 Aug 25.8	8.29	10.0	8.0–11.9	0.62	4.0 × 1.5	5.8	260 ± 10
ALMA	2017 Aug 27.0	9.43	97.5	89.5–93.5, 101.5–105.5	0.13	0.4 × 0.2	24	234 ± 32
VLA	2017 Aug 30.9	13.41	10.0	8.0–11.9	0.60	1.0 × 0.5	6.1	262 ± 20
ALMA	2017 Sep 1.8	15.33	97.5	89.5–93.5, 101.5–105.5	0.68	0.2 × 0.2	13	253 ± 16
VLA	2017 Sep 5.9	19.43	10.0	8.0–11.9	0.93	1.1 × 0.5	4.5	218 ± 11
VLA	2017 Sep 5.9	19.47	6.0	4.0–7.9	0.93	2.2 × 0.8	4.0[b]	345 ± 12
ALMA	2017 Sep 16.9	30.34	97.5	89.5–93.5, 101.5–105.5	0.68	0.2 × 0.1	14	223 ± 23
VLA	2017 Sep 25.7	39.23	6.0	4.0–7.9	1.9	1.7 × 0.7	4.4[c]	314 ± 11

Notes.
[a] At the position of the optical and X-ray counterpart. 3σ upper limits plotted in figures are $3\times$ rms.
[b] Emission detected at the counterpart position with a flux density of 19 ± 6 μJy.
[c] Emission detected at the counterpart position with a flux density of 27 ± 6 μJy.

optical counterpart[15] was also discovered by several teams, including by our group with the Dark Energy Camera (DECam; Allam et al. 2017; Coulter et al. 2017a, 2017b; Soares-Santos et al. 2017; Valenti et al. 2017; Yang et al. 2017). These detections and localization make GW170817 the first GW event with an electromagnetic (EM) counterpart, ushering in the era of multi-messenger GW–EM astronomy (LIGO Scientific Collaboration & Virgo Collaboration et al. 2017a).

Here, we present centimeter and millimeter wavelength follow-up observations of the optical counterpart, starting ≈0.6 days post-merger and extending to ≈39 days. Together with our detailed X-ray analysis (Margutti et al. 2017), we use the radio data to place tight constraints on the presence of an on- or off-axis jet. Finally, we present expectations for long-term radio emission produced by the ejecta powering the optical/near-infrared (NIR) kilonova (KN) emission (Chornock et al. 2017; Cowperthwaite et al. 2017; Nicholl et al. 2017). Our radio observations of the host galaxy, NGC 4993, are discussed in Blanchard et al. (2017).

2. Observations

We initiated radio observations of the position of the optical counterpart with the Karl G. Jansky Very Large Array (VLA; NRAO program VLA/17A-218; PI: Fong) at 9.7 GHz beginning on 2017 August 18.10 UT (13.7 hr post-merger). Subsequently, deeper VLA observations were obtained under the shared public program TTRA0001 (PI: Mioduszewski) at 1.4 days (10 GHz) and at 2.4 days (6, 10, and 15 GHz). All subsequent VLA observations, beginning at 5.5 days, were collected under program 17A-231 (PI: Alexander). The observations were performed in C, C→ B, or B configurations. We analyzed and imaged the VLA data using standard CASA routines (McMullin et al. 2007), using 3C286 as the flux calibrator and J1258–2219 as the phase calibrator. For some epochs, we also compared our reduction to the calibration performed by the automated VLA pipeline as a cross-check. For all of the detected sources, we fit the flux density and position of the emission using the imtool program within the pwkit package.[16] The reported uncertainty for detections is the uncertainty on this fit, not the image rms at the source position, which is reported separately by imtool. We use the fit uncertainty to estimate the significance of the detection. The observations are summarized in Table 1.

At the position of the optical counterpart we do not detect emission with a signal-to-noise ratio of $\gtrsim 3\sigma$ in any of our observations at <19 days. On 2017 September 2 and 3, Mooley et al. (2017) and Corsi et al. (2017) reported the emergence of radio emission with the VLA at a signal-to-noise ratio of ∼5 (summarized in Hallinan et al. 2017), which was tentatively confirmed by the Australia Telescope Compact Array (ATCA; Murphy et al. 2017). Our subsequent observations of similar duration on 2017 September 5 UT were affected by marginal weather conditions, and our initial reduction showed only a very weak peak ($\sim 2\sigma$) that did not meet our standards for detection (Alexander et al. 2017). We were subsequently able to improve the noise properties of our image, and we detect marginal emission at 6 GHz with a flux density of 19 ± 6 μJy (3.1σ significance). Given the weather impact, we conclude that this emission is likely consistent with the earlier detections reported by Mooley et al. (2017) and Corsi et al. (2017), despite the lower significance. The source is not detected to a comparable depth in our contemporaneous observations at 10 GHz, although bad weather disproportionately affects high-frequency observations so these data may suffer from flux decorrelation, as also suggested by the lower flux found for the host galaxy in this epoch. We combined our 10 GHz data taken on August 30 and September 5 and do not detect any radio emission to a 3σ limit of 11 μJy. These observations suggest that the source spectral energy distribution was optically thin at this time. We continue to detect the source in observations at

[15] This source is variously known as AT2017gfo (International Astronomical Union name), SSS17a (Coulter et al. 2017a, 2017b), and DLT17ck (Valenti et al. 2017; Yang et al. 2017).

[16] Available at https://github.com/pkgw/pwkit.

6 GHz taken on 2017 September 25 UT, with a flux density of $27 \pm 6\,\mu$Jy.

We also observed the position of the optical counterpart with the Atacama Large Millimeter/submillimeter Array (ALMA) beginning 2.4 days post-merger (programs 2016.A.00043.T and 2016.A.00046.T; PI: Alexander). Additional observations were obtained at 9.4, 15.3, and 30.3 days. The first two observations each lasted 30 minutes, while the second two lasted 1 hr each. In all cases, we used the Band 3 receiver system in wideband continuum mode, with two spectral windows of 4 GHz width centered at frequencies of 91.5 and 103.5 GHz. We calibrated and imaged the data using a custom pipeline based on CASA (McMullin et al. 2007), using the quasar B1334–127 as the bandpass and flux density calibrator. The observations are summarized in Table 1. We combined the data in both subbands and all four epochs and we did not detect emission at the optical transient position, with an image rms of 8.5 μJy at that position.

In all of our radio observations, we detect emission coincident with the optical center of the host galaxy, NGC 4993. The host emission is unresolved in the ALMA data, with a beam size of $0\farcs21$ (corresponding to $\lesssim$40 pc at a distance of 39.5 Mpc) and also appears unresolved in our VLA observations. There is no evidence for extended host radio emission at the position of the optical counterpart. For further discussion of the host emission we refer the reader to the companion paper, Blanchard et al. (2017).

3. Afterglow Constraints

The EM observations indicate that the BNS merger that produced GW170817 was accompanied by gamma-ray emission (Blackburn et al. 2017; Goldstein et al. 2017a, 2017b; Savchenko et al. 2017a, 2017b; von Kienlin et al. 2017). The shock wave produced between an SGRB jet and the surrounding medium generates a broadband synchrotron afterglow, which is expected to be the dominant source of radio emission within the first few months after the merger (Sari et al. 1998; Nakar & Piran 2011). Here we utilize the standard afterglow synchrotron model in a constant density medium (Granot & Sari 2002), as expected for a BNS progenitor. This model provides a mapping from the afterglow spectral energy distribution and temporal evolution to the isotropic-equivalent kinetic energy ($E_{\rm K,iso}$), circumbinary density (n), fractions of post-shock energy in radiating electrons (ϵ_e) and magnetic fields (ϵ_B), and the electron power-law distribution index (p), with $N(\gamma) \propto \gamma^{-p}$ for $\gamma \gtrsim \gamma_{\rm min}$, where $\gamma_{\rm min}$ is the minimum Lorentz factor of the electron distribution accelerated by the shock.

Since the jet is likely initially highly relativistic and collimated with a jet opening angle θ_j , the observed afterglow depends on the viewing angle of the observer with respect to the jet axis, $\theta_{\rm obs}$ (Granot et al. 2002). When $\theta_{\rm obs} \gtrsim \theta_j$, the emission is initially relativistically beamed away from the observer, and only becomes visible as the jet spreads and decelerates (e.g., van Eerten & MacFadyen 2012). The observed emission therefore peaks with a viewing-angle-dependent delay of days to months, when compared to the on-axis case. Below, we consider separately the constraints that our observations place on the SGRB properties in both on- and off-axis models.

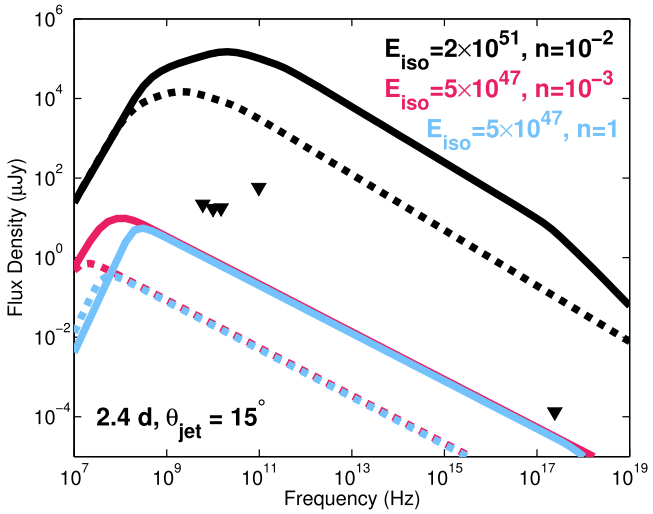

Figure 1. On-axis SGRB afterglow model spectral energy distributions at 2.4 days shown with our radio and X-ray upper limits at this epoch from the VLA, ALMA, and *Chandra* (black triangles). The red and blue curves show allowed models with $E_{\rm K,iso} = 5 \times 10^{47}$ erg for $n = 10^{-3}$ cm^{-3} and $n = 1$ cm^{-3}, respectively. The predicted emission from a "canonical" on-axis SGRB (black) is shown for comparison. We show both $\epsilon_B = 0.01$ (solid lines) and $\epsilon_B = 10^{-4}$ (dashed lines). The flux density for fixed ϵ_B is nearly density-independent at radio and X-ray frequencies for the low-energy models, as the jet has already decelerated by the time of these observations.

3.1. On-axis Afterglow Models

We first consider whether our radio observations are consistent with the emission expected from an on-axis SGRB afterglow. The detection of γ-ray emission may be indicative of an on-axis viewing angle, but the low γ-ray fluence (Goldstein et al. 2017a) implies an isotropic-equivalent kinetic energy of only $E_{\rm K,iso} \sim 5 \times 10^{47}$ erg (assuming an efficiency of $\eta_\gamma = 0.1$), orders of magnitude lower than the energies inferred for cosmological SGRBs (Berger 2014; Fong et al. 2015). From our radio observations at 2.4 days we rule out an on-axis afterglow with canonical parameters inferred from SGRBs of $E_{\rm K,iso} \sim 2 \times 10^{51}$ erg and $n \sim 10^{-2}$ cm^{-3} (Fong et al. 2015), for a wide range of values of ϵ_B (assuming $\epsilon_e = 0.1$); see Figure 1.

While all of the on-axis jets with $E_{\rm K,iso} \gtrsim 10^{48}$ erg are ruled out, we find that for $E_{\rm K,iso} \sim 5 \times 10^{47}$ erg our radio and X-ray upper limits can be accommodated for densities of $n \lesssim 1$ cm^{-3} ($\epsilon_B = 10^{-4}$–10^{-2}); see Figure 1. However, these low-density models predict fading emission and are therefore inconsistent with the radio detection at ~16–40 days and with the rising X-ray flux observed between 2.4 and 15.4 days (Margutti et al. 2017). We therefore conclude that an on-axis relativistic jet cannot explain our radio and X-ray detections.

3.2. Off-axis Afterglow Models

We next explore models in which the radio emission originates from the afterglow of a relativistic SGRB jet viewed off-axis. To constrain the value of $\theta_{\rm obs}$, we use the afterglow modeling code BOXFIT (v2; van Eerten et al. 2010; van Eerten & MacFadyen 2012) for a wide range of kinetic energies, densities, jet opening angles, observer orientations, and ϵ_B, as described in Margutti et al. (2017); we fix $\epsilon_e = 0.1$.

We first consider $p = 2.4$ and $\epsilon_B = 0.01$, the median values for SGRBs (Fong et al. 2015). We find that models with $p = 2.4$ that match the X-ray light curve (Margutti et al. 2017)

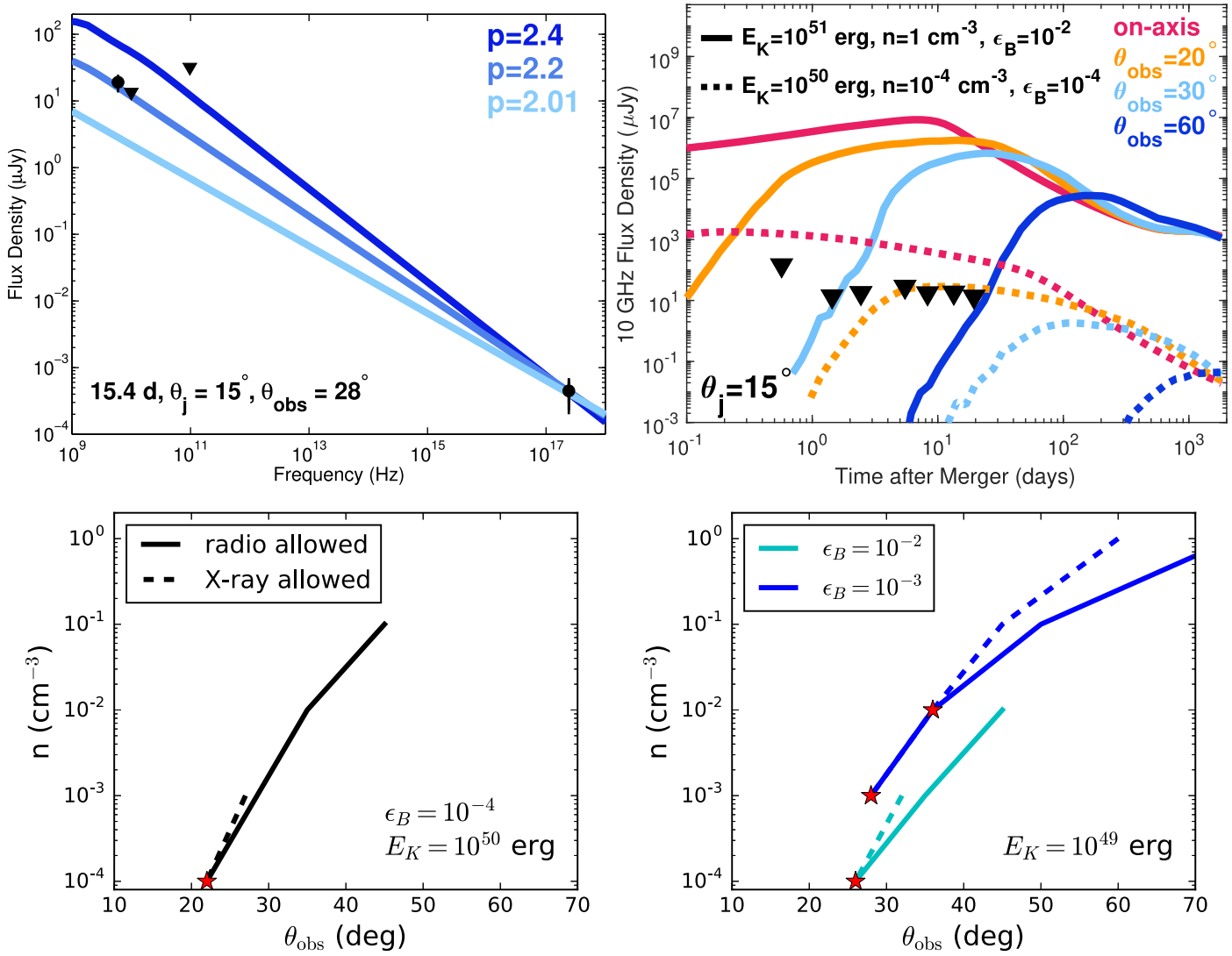

Figure 2. Constraints on model parameters from the radio and X-ray data, based on the simulation set described in Margutti et al. (2017). Upper left: three model SEDs of an off-axis 15° jet at 15.4 days that fit the X-ray emission with different values of p. We find that the models with $p > 2.2$ that match the X-ray emission over-predict the radio emission, ruling out the median value for cosmological SGRBs, $p = 2.4$. A model with $p = 2.2$ matches our radio detection at 6 GHz. Upper right: select model radio light curves explored in our simulations. Models with small $\theta_{\rm obs}$ are ruled out by our 10 GHz upper limits, while models with large $\theta_{\rm obs}$ are ruled out by our 6 GHz detections at 19 and 39 days. Models with large E_K are ruled out for all of the $\theta_{\rm obs}$ because they predict that the radio and X-ray flux densities increase faster than observed between ∼10–40 days. Bottom: the regions of parameter space allowed by our radio and X-ray observations for typical SGRB jet kinetic energies (assuming $p = 2.2$ and $\epsilon_e = 0.1$). The solid lines indicate the values of n and $\theta_{\rm obs}$ allowed by the radio observations for fixed ϵ_B and E_K. Dashed lines of the same color indicate the corresponding values allowed by the X-ray observations. Red stars mark simulations that are consistent with both the X-rays and radio observations.

consistently over-predict the radio emission at a comparable epoch (Figure 2; top left panel). On the other hand, assuming a value of $p = 2.2$ matches both the X-ray detection at 15 days and our observed weak radio emission at 6 GHz at 19 days, and is also consistent with our upper limits at 10 GHz and 97.5 GHz. All of the simulations discussed for the remainder of this paper assume $p = 2.2$, but we explore wide ranges of E_K, n, ϵ_B, and $\theta_{\rm obs}$ (Figure 2; top right panel).

When considered in isolation, the radio observations exhibit a strong degeneracy between n and $\theta_{\rm obs}$, while varying E_K and ϵ_B also causes shifts in the allowed parameter space (Figure 2; bottom panels). Observer viewing angles $\theta_{\rm obs} \lesssim 20°$ are ruled out, even for a low value of $\epsilon_B = 10^{-4}$, while the largest viewing angles require densities $n \gtrsim 1\,{\rm cm}^{-3}$. Using the constraints from the X-ray observations shifts the allowed parameter space to low densities $n \sim 10^{-4}$–$10^{-2}\,{\rm cm}^{-3}$ and tightens the viewing angle constraint to $20° \lesssim \theta_{\rm obs} \lesssim 40°$. Models with $E_K > 10^{50}$ erg and $\epsilon_B > 0.01$ are entirely ruled out. This is consistent with our modeling of the optical and NIR emission (Chornock et al. 2017; Cowperthwaite et al. 2017; Nicholl et al. 2017), which suggests that $\theta_{\rm obs} \lesssim 45°$ based on the presence of blue KN emission. The inferred values of E_K, n, and ϵ_B are well within the ranges of the observed populations of SGRBs (Fong et al. 2015, 2017). In particular, the inferred low density is consistent with GW170817's origin in an elliptical host galaxy,[17] as the expected ISM densities in elliptical galaxies are low (Fukazawa et al. 2006).

We find that all of the afterglow models that satisfy the current radio data peak on a timescale similar to the X-ray

[17] From surface brightness profile fitting, Blanchard et al. (2017) demonstrate that NGC 4993 has an elliptical morphology.

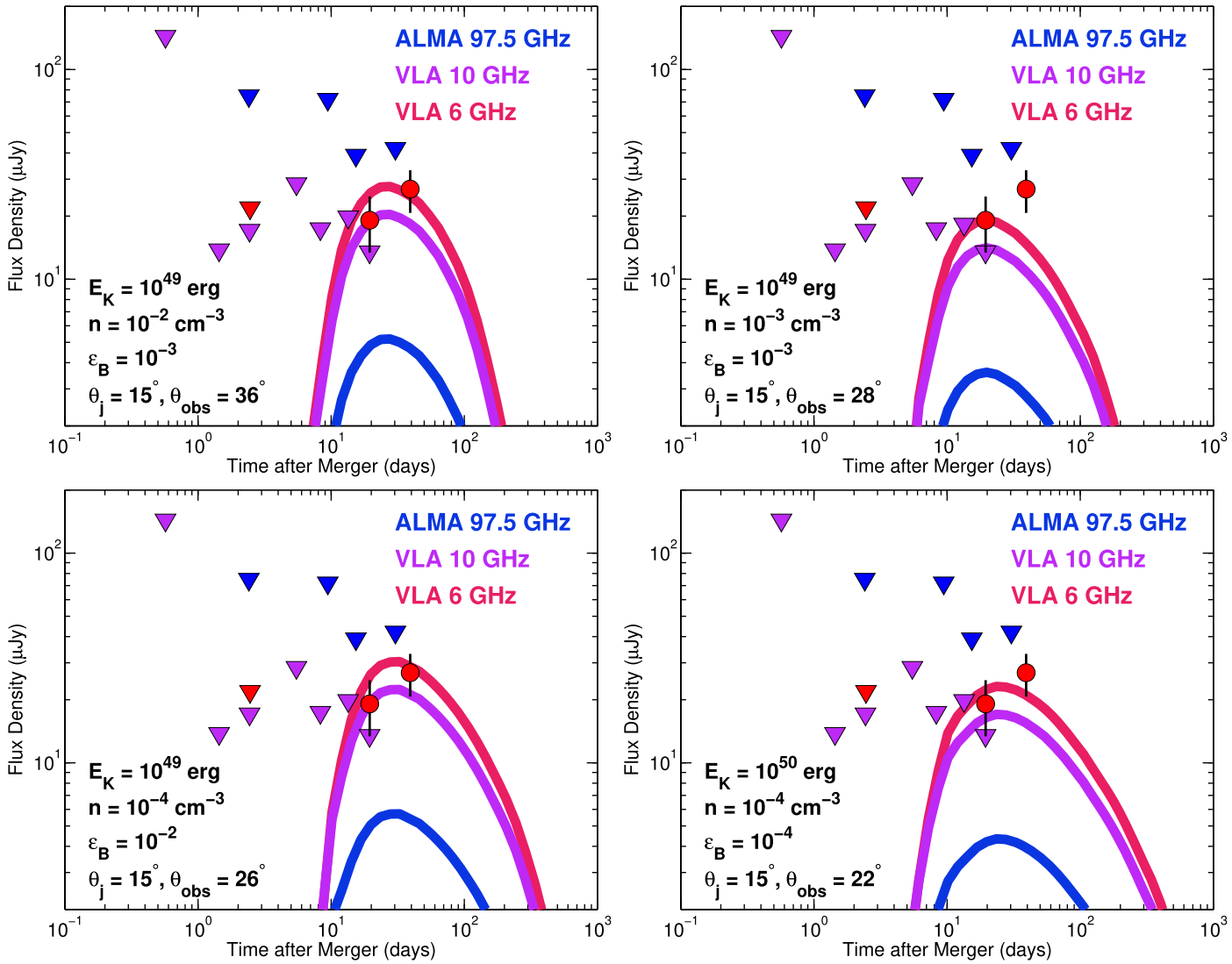

Figure 3. Simulated radio light curves for the four models also presented in Margutti et al. (2017), shown with all of our radio upper limits (triangles; 3σ) and detections (circles). The emission peaks on a timescale of ∼15–30 days, but should remain detectable at 6 GHz for weeks to months. We note that the observations at 19.2 days were taken under poor weather conditions, which can lead to flux decorrelation at high frequencies of $\gtrsim$10 GHz. Our final 10 GHz upper limit may therefore underestimate the true flux density at this epoch.

peak, ∼15–30 days (Figure 3). As the peak is fairly broad, we predict that the emission should remain detectable with the VLA for weeks to months. As GW170817 is currently too close to the Sun to be observable by X-ray and optical facilities, radio observations will remain the only way to monitor the transient emission during this time. Continued radio monitoring of GW170817 will help us further narrow down this parameter space, allowing for tighter constraints on the burst energy and circumbinary density.

4. Predictions for Future Radio Emission from the KN Ejecta

In addition to the relativistic jet, BNS mergers are also expected to generate non-relativistic ejecta, which will produce synchrotron emission at radio wavelengths once it decelerates (Nakar & Piran 2011). This is the same ejecta that initially generates the KN emission detected in the UV/optical/NIR bands. Compared to the relativistic jet, this ejecta component will decelerate on a significantly longer timescale due to its larger mass, $\approx$0.01–0.1 $M_\odot$ (Metzger & Bower 2014; Hotokezaka & Piran 2015). The radio emission from the KN ejecta is therefore expected to peak on timescales of months to years (Nakar & Piran 2011; Metzger & Berger 2012; Metzger & Bower 2014; Hotokezaka & Piran 2015). Searches for this component following a subset of cosmological SGRBs have all yielded deep non-detections, placing constraints on the kinetic energy injected of $\gtrsim 10^{51}$ erg in these events (Metzger & Bower 2014; Fong et al. 2016; Horesh et al. 2016).

For the first time, we can make specific predictions for the KN radio emission using the parameters inferred from modeling of the UV/optical/NIR emission (Chornock et al. 2017; Cowperthwaite et al. 2017; Nicholl et al. 2017). The KN emission requires two components: a "blue" component with $M_{ej} \approx 0.02\,M_\odot$ and $v_{ej} \approx 0.3c$, and a "red" component with $M_{ej} \approx 0.04\ M_\odot$ and $v_{ej} \approx 0.1c$ (Chornock et al. 2017; Cowperthwaite et al. 2017; Nicholl et al. 2017). The predicted radio emission from each component is shown in Figure 4 for a fiducial density of $n = 1 \times 10^{-3}\,\mathrm{cm}^{-3}$ (solid lines). The shaded bands indicate the full range of possible densities

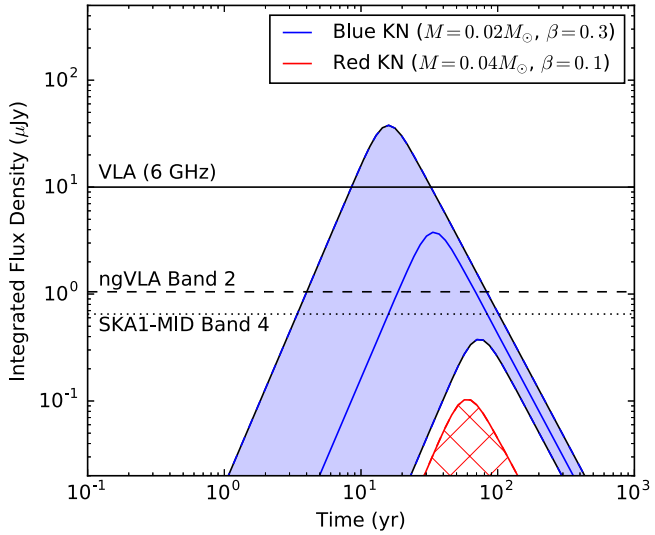

Figure 4. Radio emission predicted from decelerated KN ejecta for the two component model described in Cowperthwaite et al. (2017), assuming the density range allowed by our VLA observations, $n = 10^{-4}$–10^{-2} cm^{-3}. The blue KN component (solid blue) is detectable by the VLA at its current sensitivity for favorable parameters and is easily detectable for most of the allowed parameter range by the ngVLA and the SKA1-MID at design sensitivity, both of which are expected to be operational by the time the emission peaks. The red KN component (crosshatched red) takes longer to decelerate and is sub-dominant.

preferred by our modeling of the radio and X-ray counterparts to GW170817.

We predict that the blue KN component will dominate the radio emission at all times and will be detectable with the VLA at its current sensitivity as early as $\sim$5 years post-merger for $n = 10^{-2}$ cm^{-3}. This component dominates because of its larger kinetic energy and earlier deceleration time. For densities $n \lesssim 3 \times 10^{-3}$ cm^{-3}, the blue KN will not be detectable with the current VLA, but the next generation of sensitive radio telescopes, including ngVLA (McKinnon et al. 2016) and SKA1-MID (Carilli & Rawlings 2004) will be able to detect emission from this component for decades. Emission from the red KN component remains sub-dominant at all times. We note that radio emission from the KN ejecta-ISM interaction could begin even earlier than we have predicted if the ejecta contains a moderate tail of even faster-expanding matter with velocity $\gtrsim 0.3c$, to which optical KN observations of GW170817 are not sensitive (since its optical/UV emission would have peaked on earlier timescales of a few hours; e.g., Metzger et al. 2015; Nakar & Piran 2017).

5. Conclusions

We presented extensive radio follow-up observations of GW170817 at centimeter and millimeter wavelengths, including the earliest observations taken in these bands. Our observations rule out a typical SGRB on-axis jet ($E_{\rm K,iso} \gtrsim 10^{48}$ erg). Instead, we find that our radio observations, together with the X-ray light curve (Margutti et al. 2017), can be jointly explained as the afterglow from an off-axis relativistic jet with an energy of 10^{49}–10^{50} erg expanding into a low-density medium of $\sim 10^{-4}$–10^{-2} cm^{-3}, at an inferred $\theta_{\rm obs} \approx 20°$–$40°$. Under this interpretation, GW170817 would be the first detection of an off-axis afterglow from an SGRB, and would also be the first direct observational evidence for the launching of relativistic jets in BNS mergers. As the early optical emission is dominated by the KN ejecta, radio and X-ray observations will continue to be the best way to probe relativistic outflows in BNS mergers discovered by LIGO/Virgo, the majority of which will be off-axis (e.g., Metzger & Berger 2012).

We also use the KN ejecta properties inferred from our UV/optical/NIR data and modeling to place the first observationally motivated constraints on the predicted radio emission from the non-relativistic ejecta. Detection of this component allows for an independent measurement of the ejecta properties and the circumbinary density, but is more challenging than the detection of the afterglow due to its longevity. For GW170817, we predict emission from this component on a timescale of at least a few years post-merger. The next generation of radio telescopes will come online by the time the emission from GW170817 and future LIGO/Virgo BNS merger events reach their peak. In the upcoming era of high-sensitivity all-sky radio surveys, radio emission from BNS mergers will become a powerful piece of the EM toolkit in the new field of multi-messenger GW–EM astronomy.

The Berger Time-Domain Group at Harvard is supported in part by the NSF through grants AST-1411763 and AST-1714498, and by NASA through grants NNX15AE50G and NNX16AC22G. W.F. acknowledges support from Program number HST-HF2-51390.001-A, provided by NASA through a grant from the Space Telescope Science Institute, which is operated by the Association of Universities for Research in Astronomy, Incorporated, under NASA contract NAS5-26555. C.G. acknowledges University of Ferrara for use of the local HPC facility co-funded by the "Large-Scale Facilities 2010" project (grant 7746/2011). Development of the Boxfit code was supported in part by NASA through grant NNX10AF62G issued through the Astrophysics Theory Program and by the NSF through grant AST-1009863. B.D.M. is supported in part by NASA ATP grant NNX16AB30G. Simulations for BOXFITv2 have been carried out in part on the computing facilities of the Computational Center for Particle and Astrophysics of the research cooperation "Excellence Cluster Universe" in Garching, Germany. This paper makes use of the following ALMA data: ADS/JAO.ALMA#2016.A.00043.T and ADS/JAO.ALMA#2016.A.00046.T. ALMA is a partnership of ESO (representing its member states), NSF (USA) and NINS (Japan), together with NRC (Canada), *MOST* and ASIAA (Taiwan), and KASI (Republic of Korea), in cooperation with the Republic of Chile. The Joint ALMA Observatory is operated by ESO, AUI/NRAO and NAOJ. The National Radio Astronomy Observatory is a facility of the National Science Foundation operated under cooperative agreement by Associated Universities, Inc.

Software: CASA, Numpy, pwkit.

ORCID iDs

K. D. Alexander https://orcid.org/0000-0002-8297-2473
E. Berger https://orcid.org/0000-0002-9392-9681
W. Fong https://orcid.org/0000-0002-7374-935X
P. K. G. Williams https://orcid.org/0000-0003-3734-3587
R. Margutti https://orcid.org/0000-0003-4768-7586

References

Abbott, B. P., Abbott, R., Abbott, T. D., et al. 2016, LRR, 19, 1
Alexander, K. D., Berger, E., Eftekhari, T., Fong, W., & Margutti, R. 2017, GCN, 21851

Allam, S., Annis, J., Berger, E., et al. 2017, GCN, 21530
Berger, E. 2014, ARA&A, 52, 43
Berger, E., Price, P. A., Cenko, S. B., et al. 2005, Natur, 438, 988
Blackburn, L., Briggs, M. S., Broida, J., et al. 2017, GCN, 21506
Blanchard, P. K., Berger, E., Fong, W., et al. 2017, ApJL, https://doi.org/10.3847/2041-8213/aa9055
Carilli, C. L., & Rawlings, S. 2004, NewAR, 48, 979
Chornock, R., Berger, E., Kasen, D., et al. 2017, ApJL, https://doi.org/10.3847/2041-8213/aa905c
Corsi, A., Hallinan, G., Mooley, K., et al. 2017, GCN, 21815
Coulter, D. A. 2017a, Sci, https://doi.org/10.1126/science.aap9811
Coulter, D. A., Kilpatrick, C. D., Siebert, M. R., et al. 2017b, GCN, 21529
Cowperthwaite, P. S., Berger, E., Villar, V. A., et al. 2017, ApJL, https://doi.org/10.3847/2041-8213/aa8fc7
Fong, W., Berger, E., Margutti, R., & Zauderer, B. A. 2015, ApJ, 815, 102
Fong, W., Berger, E., Metzger, B. D., et al. 2014, ApJ, 780, 118
Fong, W., Metzger, B. D., Berger, E., & Özel, F. 2016, ApJ, 831, 141
Fong, W., Berger, E., Blanchard, P., et al. 2017, ApJL, https://doi.org/10.3847/2041-8213/aa9018
Fukazawa, Y., Botoya-Nonesa, J. G., Pu, J., Ohto, A., & Kawano, N. 2006, ApJ, 636, 698
Goldstein, A., Veres, P., Burns, E., et al. 2017a, ApJL, https://doi.org/10.3847/2041-8213/aa8f41
Goldstein, A., Veres, P., von Kienlin, A., et al. 2017b, GCN, 21528
Granot, J., Panaitescu, A., Kumar, P., & Woosley, S. E. 2002, ApJL, 570, L61
Granot, J., & Sari, R. 2002, ApJ, 568, 820
Hallinan, G., et al. 2017, Sci, https://doi.org/10.1126/science.aap9855
Horesh, A., Hotokezaka, K., Piran, T., Nakar, E., & Hancock, P. 2016, ApJL, 819, L22
Hotokezaka, K., & Piran, T. 2015, MNRAS, 450, 1430
LIGO Scientific Collaboration & Virgo Collaboration, et al. 2017a, PhRvL, https://doi.org/10.1103/PhysRevLett.119.161101
LIGO Scientific Collaboration & Virgo Collaboration 2017b, GCN, 21509
Margutti, R., Berger, E., Fong, W., et al. 2017, ApJL, https://doi.org/10.3847/2041-8213/aa9057
McKinnon, M., Chandler, C., Hibbard, J., Kern, J., & Perley, M. 2016, Proc. SPIE, 9910, 99100L
McMullin, J. P., Waters, B., Schiebel, D., Young, W., & Golap, K. 2007, in ASP Conf. Ser. 376, Astronomical Data Analysis Software and Systems XVI, ed. R. A. Shaw, F. Hill, & D. J. Bell (San Francisco, CA: ASP), 127
Metzger, B. D., Bauswein, A., Goriely, S., & Kasen, D. 2015, MNRAS, 446, 1115
Metzger, B. D., & Berger, E. 2012, ApJ, 746, 48
Metzger, B. D., & Bower, G. C. 2014, MNRAS, 437, 1821
Mooley, K. P., Hallinan, G., & Corsi, A. 2017, GCN, 21814
Murphy, T., Lenc, E., Lynch, C., et al. 2017, GCN, 21842
Nakar, E., & Piran, T. 2011, Natur, 478, 82
Nakar, E., & Piran, T. 2017, ApJ, 834, 28
Nicholl, M., Berger, E., Kasen, D., et al. 2017, ApJL, https://doi.org/10.3847/2041-8213/aa9029
Sari, R., Piran, T., & Narayan, R. 1998, ApJL, 497, L17
Savchenko, V., Ferrigno, C., Kuulkers, E., et al. 2017a, ApJL, https://doi.org/10.3847/2041-8213/aa8f94
Savchenko, V., Mereghetti, S., Ferrigno, C., et al. 2017b, GCN, 21507
Soares-Santos, M., Holz, D. E., Annis, J., et al. 2017, ApJL, https://doi.org/10.3847/2041-8213/aa9059
Soderberg, A. M., Berger, E., Kasliwal, M., et al. 2006, ApJ, 650, 261
Valenti, S., Sand, D. J., Yang, S., et al. 2017, ApJL, https://doi.org/10.3847/2041-8213/aa8edf
van Eerten, H., Zhang, W., & MacFadyen, A. 2010, ApJ, 722, 235
van Eerten, H. J., & MacFadyen, A. I. 2012, ApJ, 751, 155
von Kienlin, A., Meegan, C., & Goldstein, A. 2017, GCN, 21520
Williams, P. K. G., Clavel, M., Newton, E., & Ryzhkov, D. 2017, pwkit: Astronomical utilities in Python, Astrophysics Source Code Library, ascl:1704.001
Yang, S., Valenti, S., Sand, D., et al. 2017, GCN, 21531